Initial Steps toward the Development of Grafted Ionic Liquid Membranes for the Selective Transport of CO 2

Marie-Alix Pizzoccaro-Zilamy, Martin Drobek, Eddy Petit, Cédric Totée,
Gilles Silly, Gilles Guerrero, Matthew Cowan, Andre Ayral, Anne Julbe

Initial steps towards the development of Grafted Ionic Liquid Membranes for the selective transport of CO$_2$

Marie-Alix Pizzoccaro-Zilamy,[†,§] Martin Drobek,[†] Eddy Petit,[†] Cédric Totee,[‡] Gilles Silly,[‡] Gilles Guerrero,[‡] Matthew G. Cowan,[†,ǁ] André Ayral,[†] and Anne Julbe[†,]*

[†]Institut Européen des Membranes, UMR-5635 CNRS-UM-ENSCM, Université de Montpellier, Place Eugène Bataillon, F-34095 Montpellier cedex 5, France. [‡]Institut Charles Gerhardt, UMR-5253 CNRS-UM-ENSCM, Université de Montpellier, Place Eugène Bataillon, F-34095 Montpellier cedex 5, France.

ABSTRACT

This work reports on a promising strategy for the development of novel Grafted Ionic Liquid Membranes (GILMs) in which phosphonate-based ILs are confined within the pores of a mesoporous γ-Al$_2$O$_3$ ceramic membrane by chemical grafting. The influence of both the

1

chemical nature (*i.e.,* alkyl versus ether) of the organic spacer chain and the presence of phosphonate coupling functions were evidenced as crucial parameters influencing CO_2 transport through the membranes. The effectiveness of the grafting procedure yielding GILMs was clearly demonstrated by FTIR and HR-MAS NMR and attractive membrane performance was evidenced through both the CO_2/N_2 ideal selectivity (~140) and CO_2 permeability (~130 Barrer).

1. INTRODUCTION

In the past few decades, membrane-based separation processes have undergone enormous progress and have potential as systems for the post-combustion CO_2 capture technologies. Research has focused on the synthesis of membranes and investigation of their performance (*selectivity vs flux*) and stability (*i.e. high temperature, high pressure*) in order to obtain a continuous system that is competitive with other CO_2 capture methods (*i.e. absorption by amine-based solvents or ammonia, adsorption by solids, calcium cycles or cryogenics*).[1,2]

Confinement of Ionic liquids (ILs) into porous ceramic supports to prepare Supported Ionic Liquid Membranes (SILMs) has gained attention in recent years because of the unique properties of ILs such as a limited vapor pressure, coupled with good chemical and thermal stability[1-3]. Moreover, reactive ILs interact strongly and reversibly with CO_2, making SILMs attractive systems for continuous gas separation applications. Conventional SILMs contain an IL immobilized by capillary forces within the pores and eventually on the support top surface. In spite of their good CO_2 separation performance[4-6], such membranes are mechanically unstable as the IL can be easily displaced from most support materials under a pressure gradient.

To overcome these issues a new generation of SILMs has been recently developed by surface modification of mesoporous or microporous ceramic supports using functional ILs.[7] Indeed,

covalent linking of ILs is generally easy on many ceramic oxide materials whose surface composition (*i.e.,* hydroxyl-groups, metallic sites) favors reactions with specific IL functional groups (*i.e., trimethoxysilyl-, thiol-, ether-, carboxylic acid-group*).[8] Despite the cost and relative brittleness of porous ceramic supports compared to polymeric ones, the grafting of ILs on these supports remains an attractive strategy to circumvent IL leaching, minimize the required IL amount during membrane synthesis and guarantee good thermo-mechanical stability for the final membranes on a large operational pressure range.[8] The preparation of these **Grafted Ionic Liquid Membranes (GILMs)** requires a precise control of the ionocovalent bonds formation between the coupling function of the IL and the surface functional groups of the ceramic support. Up to now it has been scarcely studied in the literature.[7] The present work focuses on the preparation of new GILM series in which selected ILs are confined within the pores of a mesoporous γ-Al_2O_3 ceramic membrane support by chemical grafting using a dialkylphosphonate coupling function. Hence, this work represents a fundamental step towards the development of phosphonate-based GILMs.

According to the literature, there are several possible bonding modes for phosphonate coupling molecules on an oxide surface.[9] In the case of phosphonyl imidazolium-based ILs, the possible bonding modes can be mono-, bi- or tri-dentate. We have recently demonstrated that the use of the imidazolium diethylphosphonate coupling molecule allowed an effective control of the grafting reaction on γ-Al_2O_3 surface by using either prolonged or high temperature grafting.[10] Thanks to a series of specific techniques, we have demonstrated that the grafting procedure enables the immobilization of the phosphonate-based ILs on the γ-Al_2O_3 grain surface with homogeneous and controlled grafting density.

Herein, we explore the influence of the chemical nature (*i.e.,* alkyl versus ether) of the organic spacer and phosphonate coupling functions on CO_2 solubility of pure ILs, and CO_2 transport on grafted γ-Al_2O_3/IL membranes. The studied ILs are composed of 1-methylimidazolium as cation core connected through an organic spacer (*i.e., propyl chain or oligo(ethylene glycol) chain*) to a diethyl phosphonate ester coupling function, while the anion was based on bis(trifluoromethanesulfonylimide) (Tf_2N^-) (Figure 1). A special attention was devoted to the grafting reaction conditions as well as the demonstration of the ILs grafting onto the γ-Al_2O_3 support through a set of characterization techniques. The CO_2/N_2 ideal selectivity and CO_2 permeability were also investigated in detail. The attractive performance of the as-prepared GILMs was evidenced through both the CO_2/N_2 ideal selectivity (~140) and CO_2 permeability (~130 Barrer).
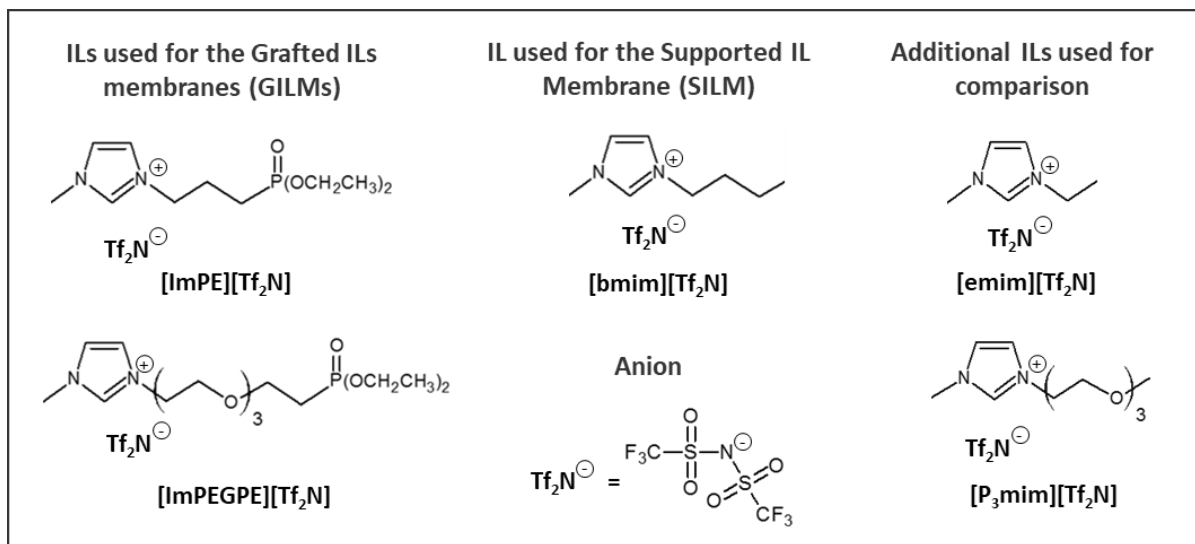

Figure 1. Representation of the compounds discussed in this study. Compounds [ImPE][Tf_2N] and [ImPEGPE][Tf_2N] are phosphonate-based ILs. [bmim][Tf_2N] and [emim][Tf_2N] are conventional ILs and [P$_3$mim][Tf_2N] is a functionalized IL.

2. EXPERIMENTAL SECTION

2.1 Materials and Instrumentation.

Methylene chloride (CH_2Cl_2), acetone, ethanol and tetrahydrofuran (THF) were purchased from Sigma-Aldrich. The solvents were used as received, except for THF which was dried on a silica-alumina column (PureSolv- InnovativeTechnology). Reagent grade solvents and ultrapure water were used in all reactions. Triethylphosphite (98%), and 1-methylimidazole (≥99%) were purchased from Sigma-Aldrich and used as received. 1,3-dibromopropane (98%) was provided by Acros Organics. The 1-butyl-3-methylimidazolium bis(trifluoromethanesulfonimide) ([bmim][Tf$_2$N], **Figure 1**), was purchased from Solvionic. The diethyl 2–(2–(2–(2–bromoethoxy)ethoxy)ethoxy)ethylphosphonate was purchased from Sikemia.

Porous alumina discs ($\emptyset$ = 25 mm, 1 mm thick) with a γ-Al_2O_3 top-layer (3−5 nm pore size) were provided by Fraunhofer-IKTS (Germany) and used as membrane supports for the preparation of IL-based membranes (GILMs and SILM). Details of the porous ceramic support structure are available in the *Supporting Information*.

For gas permeation measurements CO_2, CH_4, and N_2 were purchased from Air Products with high purities (99+ %).

^{1}H, ^{13}C, ^{31}P, and ^{19}F liquid NMR spectra were recorded using a Bruker 300 MHz NMR spectrometer equipped with a 5 mm QNP probe at respective frequencies of 300.13, 75.42, 121.49 and 282.4 MHz.

Mass Spectra were measured on a Synapt G2-S mass spectrometer (Waters) by using the electrospray ionization (ESI) mode. Elemental analyses were performed using an Elementar Vario Micro Cube instrument.

The volumetric mass density of the [ImPE][Tf$_2$N] and [ImPEGPE][Tf$_2$N] ILs were measured at 22°C with volumetric flasks of either 2 or 5 mL and weight measurements were realized on a custom-made installation (more details are provided in *Supporting Information*).

The viscosity of phosphonate-based ILs was measured using a Stabinger viscosimeter at 10, 20, 30, and 40°C.

SEM images were obtained with Hitachi S-4800 field-emission scanning electron microscope (Japan) using an accelerating voltage of 2 kV. Samples were metallized with platinum to favor charge release. The weight % of phosphorus in the samples was determined by EDX using a Zeiss SEM (EVO HD15) at 10 kV with Oxford instruments software.

FTIR spectra were obtained with a Perkin-Elmer Spectrum 2 spectrophotometer. Spectra were recorded in the 4000-400 cm^{-1} range using 4 scans at a nominal resolution of 4 cm^{-1} in ATR mode (γ-alumina spectrum was used as background).

High Resolution-MAS NMR experiments were carried out on a Varian VNMRS 600 MHz spectrometer equipped a wide bore magnet (B$_0$=14.1T), ^{2}D lock and Z gradients together with a broadband ^{15}N-^{31}P 2 channels 4 mm Fast Nano probe. Experiments were performed at 20°C. The probe-head was precooled to 20°C before loading the sample into the instrument. The sample/probe temperature was maintained throughout the experiment (±0.1 °C) via a variable temperature control unit. The sample spinning rate was 4 kHz. A single pulse sequence was used with pulse durations corresponding to flip angle of 90° pulse for ^{1}H and ^{19}F and 30° for ^{31}P. In the latter case ^{1}H high power decoupling was also used during acquisition period. For ^{1}H the pulse length was 10.25 μs, a recycling delay of 5 s was used and 16 transients were co-added. For ^{19}F and ^{31}P these parameters were respectively 6.25 and 3.38 μs for the pulse length, 5 and 30 s for the recycle delay, 16 and 3 200 for the number of transcients.

Prior to HR-MAS NMR experiments, the grafted IL membrane sample GILM(1), was broken in pieces and dried for 1h at 80°C under vacuum to remove water excess. Membrane pieces were placed into a quartz insert and drops of DMSO (used as Deuterium solvent) were added. The as-prepared sample was inserted into to a 4 mm zirconia HR-MAS rotor.

2.2. Synthesis of the phosphonate-based ILs.

2.2.1. *1-methyl-3-ethyl-imidazolium* *bis(trifluoromethanesulfonimide)* (abbreviated **[emim][Tf$_2$N], Figure 1**) was synthesized as described in the literature.[11]

2.2.2 *1-methyl-3-(3-(diethylphosphinyl)propyl)-imidazolium* *bromide* (**[ImPE][Br]**) was synthetized by applying the same synthesis protocol as in our previous publication.[10]

2.2.3. *1-methyl-3-(3-(diethylphosphinyl)propyl)-imidazolium bis(trifluoromethanesulfonimide),* (**[ImPE][Tf$_2$N], Figure 1**) was synthetized in a round bottom flask as follows: 18.8 g (55.13 mmol) of 1-methyl-3-(3-(diethylphosphinyl)propyl)-imidazolium bromide were dissolved in 50 mL of absolute ethanol. Then Lithium bis(trifluoromethanesulfonimide) (23 g, 80 mmol) was added to the solution a white precipitate formed. The reaction mixture was stirred for 24 h and then concentrated under reduced pressure. 30 mL of distilled water were added under stirring to the remaining suspension to solubilize the solid part and the resulting solution was extracted with 30 mL of CH$_2$Cl$_2$. The CH$_2$Cl$_2$ phase was washed three times with distilled water (3 x 30 mL) and the organic phase extracted. Finally, CH$_2$Cl$_2$ was removed under reduced pressure (0.1 bar) at 60°C for 2h to yield 20.8 g (38.5 mmol, 70%) of **[ImPE][Tf$_2$N]** as a light yellow viscous oil. To avoid water exposure, the IL was stored under high vacuum in a schlenk flask equipped with high vacuum valves. ^{1}H NMR (300 MHz, DMSO, δ(ppm)): 9.07 (s, 1H, N–CH–N); 7.76 (s, 1H, N–CH); 7.69 (s, 1H, N–CH); 4.20 (t, 2H, CH$_2$–N); 3.98 (m, 4H, O–CH$_2$–CH$_3$); 3.831 (s, 3H,CH$_3$–N); 2.1-1.68 (m, 4H, CH$_2$–CH$_2$–P); 1.22 (t, 6H,O–CH$_2$–CH$_3$). ^{13}C NMR (75.432 MHz,

DMSO, δ(ppm)): 136.87; 126; 123.78; 122.23; 121.73; 117.47; 113.2; 61.29; 61.2; 49.07; 48.81; 35.78; 23.27; 23.22; 22.36; 20.5; 16.23; 16.15. ^{31}P RMN (121.442 MHz, DMSO,, δ(ppm)): 30.39. ^{19}F NMR (170.385 MHz, DMSO, δ(ppm)): -78.71. Elemental analysis calculated (%): C (38.7); H (6.5); N (8.0); S (12.2); found: C (26.29); H (3.54); N (9.16); S (13.35). Exact mass calculated for ESI(+), (m/z): 261.1368; found: 261.1368. Exact mass calculated for ESI(-), (m/z): 279.9173; found: 279.9178.

2.2.4. 1-methyl-3-(3-(diethylphosphinyl) 2–(2–(2–(2–ethoxy)ethoxy)ethoxy)ethyl)-imidazolium bromide (**[ImPEGPE][Br]**) was synthetized by adding diethyl-(2-{2-[2-(2-bromo-ethoxy)-ethoxy]-ethoxy}-ethyl)phosphonate precursor (6.12 g, 16.2 mmol) to 1-methylimidazole (1.25 g, 15.2 mmol). The mixture was stirred at 110°C for 40 minutes under argon resulting in **[ImPEGPE][Br]** as yellow liquid with a 99% yield (15.2 mmol, 6.96g). ^{1}H NMR (300 MHz, CDCl$_3$, δ (ppm)): 10.4 (s, 1H, N$^+$-C*H*-N); 7.69 (s, 1H, =C*H*); 7.4 (s, 1H, =C*H*); 4.63 (t, 2H, N$^+$-CH$_2$); 4.12 (q, $^{3}J_{H-H}$ = 9.81 Hz, 4H, OC*H$_2$*CH$_3$); 4.07 (s, 3H, CH$_3$-N$^+$); 3.90 (m, 2H, N$^+$CH$_2$C*H$_2$*); 3.75 – 3.63 (massif, 12H, CH$_2$-O); 2.11 (m, 2H, PC*H$_2$*CH$_2$); 1.35 (t, 6H, OCH$_2$C*H$_3$*). ^{13}C NMR (75.432 MHz, CDCl$_3$, δ (ppm)): 137.917; 123.601; 122.605; 70.35; 70.284; 70.245; 70.148; 69.031; 65.105; 61.75; 49.75; 36.586; 27.844; 25.996; 16.476; 16.397. ^{31}P NMR (121.442 MHz, CDCl$_3$, δ(ppm)): 28.54.

2.2.5. 1-methyl-3-(3-(diethylphosphinyl) 2–(2–(2–(2–ethoxy)ethoxy)ethoxy)ethyl)-imidazolium bis(trifluoromethanesulfonimide) (**[ImPEGPE][Tf$_2$N], Figure 1**). A solution of 9.77 g (21.25 mmol) of 1-methyl-3-(3-(diethylphosphinyl)2–(2–(2–(2–ethoxy)ethoxy)ethoxy)ethyl)-imidazolium bromide in 30 mL of distilled water was first prepared. Then lithium bis(trifluoromethanesulfonimide) (6.6 g, 22.93 mmol)) was added resulting in the formation of a white precipitate. The reaction mixture was stirred for 1h and after decantation a yellow oil phase

and a white aqueous phase appeared. The two phases were separated and the yellow oil was washed three times with distilled water (3 x 20 mL). Traces of water were removed under reduced pressure (0.1 bar) at 80°C for 3h to yield 10.45 g (15.8 mmol, 74%) of **[ImPEGPE][Tf$_2$N]** as a light yellow viscous oil. To avoid water exposure, the IL was stored under high vacuum in a schlenk flask equipped with high vacuum valves.^{1}H NMR (300 MHz, DMSO, δ(ppm)): 9.04 (s, 1H, N$^+$-CH-N); 7.71 (s, 1H, =CH); 7.69 (s, 1H, =CH); 4.33 (t, 2H, N$^+$-CH$_2$); 3.98 (q, $^3J_{H-H}$ = 9.81 Hz, 4H, OCH$_2$CH$_3$); 3.86 (s, 3H, CH$_3$-N$^+$); 3.76 (t, 2H, N$^+$CH$_2$CH$_2$); 3.61 – 3.48 (m, 12H, CH$_2$-O); 2.11 (m, 2H, PCH$_2$CH$_2$); 1.21 (t, 6H, OCH$_2$CH$_3$). ^{13}C NMR (75.432 MHz, CDCl$_3$, δ(ppm)): 135.95; 124.98; 122.52; 121.83; 120.76; 116.49; 112.27; 69.81; 69.70; 69.53; 67.28; 63.56; 60.15; 60.07; 47.91; 34.87; 26.04; 24.23; 15.42; 15.34. ^{31}P NMR (121.442 MHz, DMSO, δ(ppm)): 28.66. ^{19}F NMR (270.385 MHz, DMSO, δ(ppm)): -78.73. Elemental analysis calculated (%): C (33.5); H (5.0); N (4.0); S (9.9); found: C (30.97); H (4.29); N (8.65); S (10.61). Exact mass calculated for ESI(+), (m/z): 379.1998; found: 379.1995. Exact mass calculated for ESI(-), (m/z): 279.9173; found: 279.9177.

2.3. Gas solubility measurements. On the basis of the experimental set-up designed by R. Noble and co-workers,[12] we have developed a system capable to measure single-gas solubility applying the isochoric saturation method. This home-made system (**Figure S2.a**) used for measuring gas solubilities in ILs was specifically designed to fit into a temperature controlled chamber (Sartorius Certomat HK). Two experiments could be performed at the same time by using two stainless steel cells with respective volumes of 105 and 57 cm^3. Each cell top is sealed via a copper gasket (Neyco, CF CU 39) and connected to a reference cell of 15 cm^3 (Swagelok) used for gas injection. The instrument was composed of VCR connections with aluminum gasket (Swagelok). Pressure gauges (one PA33X/0-10 bars and two PA33X/0-3 bars, Keller) were

interfaced with home-made software for automated data collection. The upper chamber was made of stainless steel with a 1000 cm^3 volume capacity. The temperature of the installation was continuously controlled and adjusted (+/- 2% for the heating circuit). Before any measurement, both the system and the ILs were well outgassed overnight under vacuum (5.0×10^{-5} mbar) using a turbomolecular pump (Leybold, Turbovac 50). To verify the system integrity (connections, valves), the apparatus was progressively filled with He in order to measure possible leaks (Alcatel ASM series Leak detectors). Prior to measurements, the volumes of each part of the apparatus were carefully determined with He, using the ideal gas law. Gas solubility values were measured as follows: the considered IL ($\approx$10-20 mL) was introduced in the stainless steel cell with a stir bar (of known volume), and the system was sealed. The IL was degassed for 10 h (vacuum pressure of $5x10^{-5}$ mbar) before injecting the feed gas to both the upper chamber and the reference cell at pressures between 7.5 and 8.5 bars. Before starting the experiment, the gas was allowed to expend in the apparatus for 30 minutes. Finally, the reference cell was isolated from the upper chamber. The automated data collection started once the valve connecting the stainless steel and the reference cell was opened. The pressure decrease (resulting from gas absorption into the IL) was monitored over time (**Figure S2.b**). Depending on the type and quantity of the ILs, the equilibrium was reached after 1 to 3h. The CO_2 solubility data measured for [emim][Tf$_2$N] (used as standard) were in line with those published in literature (*i.e.,* H_{CO2} at 42 atm).[11]

2.4. Preparation of the [bmim][Tf$_2$N]-Supported Ionic Liquid membrane (SILM). The [bmim][Tf$_2$N]-SILM sample was prepared by placing the pristine alumina ceramic support disc into a glass container. IL was subsequently deposited on the γ-Al$_2$O$_3$ top-layer with the help of a 10 µL micropipette to ensure a complete support wetting. Finally, the excess of IL was removed

from the surface with blotting paper. Samples were weighted with analytical balance before and after the coating procedure (43.8 mg (31 μL) of [bmim][Tf$_2$N]).

2.5. Preparation of the Grafted Ionic Liquid Membranes (GILMs) samples. All the GILM samples were prepared using the same experimental protocol. Experiments were conducted both on entire alumina discs and small companion samples. The entire discs were used for dynamic membrane characterization (gas permeation) while the companion samples were used for physico-chemical characterization. The grafting solution was prepared by dissolving different proportions (**Table 1**) of the IL (either **[ImPE][Tf$_2$N]** or **[ImPEGPE][Tf$_2$N]**) in 20 mL of an ethanol-water solution (60/40 vol.%). Then, the grafting solution was added to a 120 mL autoclave containing both an entire ceramic disc and its companion sample. Finally, the autoclave was closed with a PTFE cap, sealed and heated at 130°C according to the grafting reaction times reported in **Table 1**. The resulting Grafted Ionic Liquid Membranes (GILM(1) and GILM(2)) and their companion samples were washed by immersion in 20 mL of ethanol-water solution (60/40 vol.%) to remove the excess of ILs from the surface. Samples were then dried for 17h at 70°C and weighted at room temperature before and after the coating procedure.

Table 1. Details of the reaction conditions for [bmim][Tf$_2$N]-SILM, GILM(1) and GILM(2) samples preparation. *from EDX analysis.*

Sample	IL formulation	Grafting reaction time (h)	ILs quantity mmol	Atomic % ratio P:S*
SILM	[bmim][Tf$_2$N]	-	≈ 0.1	-
GILM(1)	[ImPE][Tf$_2$N]	30	14.4	1:1.5
GILM(2)	[ImPEGPE][Tf$_2$N]	40	6.1	1:1.5

2.6. Single gas permeation measurements. The permeability, P_i*, of a single gas "i" through

a material reflects the ability of the material to dissolve this gas (solubility, S_i) and the ability of

the gas to diffuse through this material (diffusivity, D_i). Hence, the permeability P_{i*} of a gas "i"

through a given dense material corresponds to the product of the diffusivity coefficient, D_i, and

the solubility coefficient, S_i (Eq 1.).[13,14]

$$P_i^* = S_i . D_i \qquad (1)$$

The permeance of single gases (N_2, CH_4 or CO_2) through both pristine γ-Al_2O_3 membrane

support and IL-based membranes was measured using a stainless steel permeation module. A

schematic representation of the experimental set-up is depicted in **Figure S3**. The feed gas

pressure was set at 3.5 bar (P_{up}) through a pressure transducer while the permeate compartment

was connected to atmospheric pressure (P_{atm}). The tightness between the internal and external

compartments was ensured by two PTFE seals surrounding the alumina ceramic support. The

flow rate of the permeating gas was measured with a bubble flow meter. The permeance (Π_A) of

a single gas A (*i.e.,* N_2, CO_2) through the membrane ($mol.m^{-2}.s^{-1}.Pa^{-1}$) corresponds to the ratio of

the gas molar flux J_A ($mol.s^{-1}.m^{-2}$) (*i.e.,* molar flow per membrane unit area) to the applied

transmembrane pressure ($\Delta P = P_{up} - P_{atm}$), as shown in Eq. 2.

$$\Pi_A = \frac{J_A}{\Delta P} \qquad (2)$$

The effective membrane area exposed to the gas was 2.84 cm². Prior to any measurement,

membranes were outgassed under vacuum for 1h at 100°C. The ideal CO_2/N_2 selectivity was

calculated from the ratio of the CO_2 and N_2 single gas permeance. The detection limit of the gas

permeation set-up was 1×10^{-11} $mol.m^{-2}.s^{-1}.Pa^{-1}$. In the case of N_2-tight membrane, the latter

value was used to estimate the CO_2/N_2 ideal selectivity. The CO_2 single gas permeability

(expressed in Barrer) was calculated from the CO_2 permeance and the membrane thickness (estimated from SEM/EDX observations).

3.RESULTS AND DISCUSSION

Aiming at the development of hybrid GILMs membranes, composed of a functional IL chemically grafted and nanoconfined in the pores of a ceramic support, the diethylphosphonate ester group was selected as the reactive coupling function to be tethered to the support surface and linked to the cationic part of the IL by an organic spacer (as sketched in **Figure 1).** Alkylphosphonate ester are interesting coupling functions allowing a controlled surface grafting, while excluding the formation of bulk phases even after prolonged reaction time.[15] The most suitable cations, anions and organic spacers (functional groups) have been selected and are shown in **Figure 1**. The bis(trifluoromethanesulfonimide) has been chosen as an anion because of its chemical stability and ability to easily solubilize CO_2. The commonly used 1-methylimidazolium was preferred as a cation and was used as a reference for comparison with 1,3-dialkylimidazolium-based ILs already reported in the literature for gas separation applications.[16,17] Different organic spacers were chosen: a propyl and an oligo(ethylene glycol) chain. The former allows a rapid comparison with conventional alkylimidazolium-based ILs (*i.e.,* [emim][Tf$_2$N] or [bmim][Tf$_2$N]), while for the oligo(ethylene glycol) chain in IL Bara *et al.*[12] demonstrated CO_2/N_2 or CO_2/CH_4 selectivity values which are 30 to 75% higher than those measured for the same ILs without any functional group. The synthesis procedure for the preparation of phosphonate-based ILs was adapted from the works of Mu *et al.*[18,19] and Rout *et al.*[20] It corresponds to the direct quaternization of 1-methylimidazole using phosphonate based reagents followed by an anion exchange reaction.

3.1. Single-gas solubilities and derived ideal solubility selectivities of pure phosphonate-based ILs.

Gas transport through Supported Ionic Liquid Membranes (SILMs) is governed by a solution-diffusion mechanism. The gas solubility plays a more important role than the diffusivity in determining the CO_2/N_2 or CO_2/CH_4 selectivity values in SILMs. We postulated that the same trend should be observed in the Grafted Ionic Liquid Membranes (GILMs). Gas permeability, solubility, and diffusivity of analogous ILs without any coupling function, such as [hmim][Tf_2N], have already been reported in the literature. These ILs were studied as bulk liquids[21-23] or as selective layers in SILM based on either polymer[24] or ceramic matrices[6]. However, in the literature there are no reports about the gas performance of ILs bearing a diethyl phosphonate coupling function, neither as bulk liquids (*i.e. with a free coupling function*) nor in hybrid materials (*i.e. with the coupling function anchored to the solid surface*). Experimental values of the solubility coefficients of single gases in the bulk liquid allow valuable prediction of the membrane efficiency for gas mixture separations. Moreover, these values are useful to compare the behavior and performance of a free IL and its nanoconfined (grafted) counterparts. The solubility of singles gases (CO_2, N_2 and CH_4) in phosphonate-based ILs were measured at 20, 30 and 40°C and the solubility selectivity was estimated from these measurements. In order to compare the values with the data of conventional-ILs, [bmim][Tf_2N] and [P_3mim][Tf_2N] (**Figure 1**) were selected as standards. When no data were available, [emim][Tf_2N] was used to allow a comparison with the literature (**Figure 1**). Details about the principle of gas solubility measurements, the values of single gas solubility (S_{gas}), Henry constants (*H(atm)*), and molar gas fractions (x_{gas}) for both CO_2 and N_2 at 20, 30, and 40°C for the phosphonate-based ILs developed in this work (*i.e., [ImPE][Tf_2N] and [ImPEGPE][Tf_2N]*) are given in *Table S3*. As expected the

absorption process is exothermic, *i.e.,* the relative quantity of CO_2 absorbed per amount and volume of phosphonate-based IL decreases as the temperature increases. As shown in **Figure 2.A.**, these results follow similar trends to those observed for both [emim][Tf_2N] and [P_3mim][Tf_2N]. Specifically, [ImPEGPE][Tf_2N] presents a 13% lower CO_2 solubility (mol.L^{-1}.atm^{-1}) at 40°C compared to [P_3mim][Tf_2N]. However, the situation is different at 20°C, the CO_2 solubility values of both [ImPE][Tf_2N] and [ImPEGPE][Tf_2N] are 8% higher than the CO_2 solubility of [emim][Tf_2N] at 25°C. Thus, these first results suggest that the CO_2 solubility properties of the phosphonate-based ILs are more attractive at lower temperature. Concerning the N_2 solubility, the amount of gas dissolved is significantly higher in [ImPEGPE][Tf_2N] compared to [ImPE][Tf_2N] (respectively 0.015 and 0.0052 mol.L^{-1}.atm^{-1} at 20°C). The N_2 Henry constants measured for the phosphonate-based ILs are low in comparison with those of [emim][Tf_2N] and [P_3mim][Tf_2N] ILs, indicating that significantly higher amount of N_2 molecules are dissolved in the studied phosphonyl ILs. Nevertheless, the N_2 solubility is still low compared to the CO_2 solubility and remains nearly constant when the temperature increases. Regarding the CH_4 solubility, the measured value reveals relatively high absorption of CH_4 compared to conventional ILs, suggesting that the phosphonate-based ILs are not good candidates for the CO_2/CH_4 separation (*e.g., H_{CH4} of [ImPE][Tf_2N]*) *is 233 atm at 30°C, and 350 atm for [hmim][Tf_2N] at 25°C* [11]). In the case of [ImPEGPE][Tf_2N], no reproducible results were obtained.
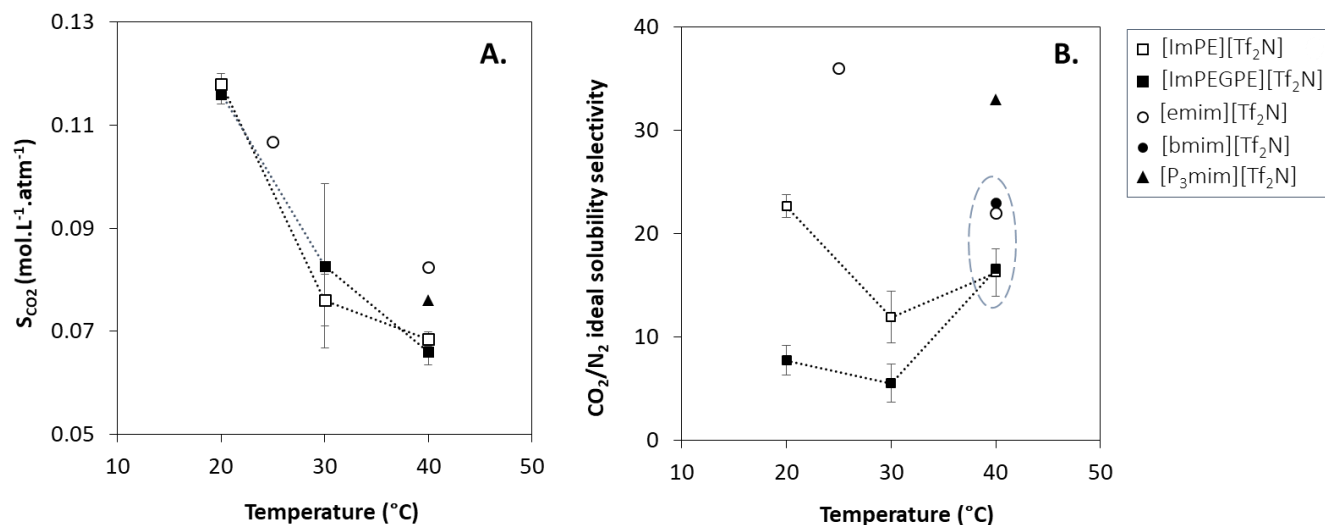
Figure 2. Evolution of **A.** CO_2 solubility, and **B.** CO_2/N_2 ideal solubility selectivity, vs. temperature for a series of ILs. (doted circle in B. represents the area to which the ideal CO_2/N_2 selectivity values converge).

Solubility measurements were used to estimate the ideal solubility selectivities (Table S4) of the phosphonate-based ILs, by calculating the ratio of S_{CO2}, (*i.e.,* solubility of CO_2) on S_j, (*i.e.,* solubility of either N_2 or CH_4). Table S4 and **Figure 2.B.** indicate that at high temperatures, the ideal S_{CO2}/S_{N2} selectivity of all the ionic liquids reported in the literature converge to a value in the range 16-23 (*except [P₃mim][Tf₂N] which is known to feature higher S_{CO2}/S_{N2} selectivity values of ~33*).[11] Indeed, the trend observed for the evolution of CO_2/N_2 ideal solubility vs. temperature obeys to thermodynamic laws. For low-solubility gases (*i.e., N₂, CH₄, H₂ having high Henry constant values*), solubility increases with increasing temperature, corresponding to a positive enthalpy and entropy. While, for gases with higher solubilities (*i.e., CO₂, SO₂ having lower Henry constant*), solubility is expected to decrease with increasing temperature, corresponding to negative enthalpy and entropy changes.[11] It must be also noted that at 20°C, [ImPE][Tf₂N] displays a S_{CO2}/S_{N2} selectivity of 23 ± 1.1, which is much higher than the value

measured for [ImPEGPE][Tf$_2$N], *i.e.*, $S_{CO2}/S_{N2} = 8 \pm 2.7$. This result fits with the behavior of the [C$_x$mim][Tf$_2$N] family of ILs, where the cation with the shortest chain length, [emim][Tf$_2$N], yields the lowest CO_2 solubility and the highest CO_2/N_2 selectivity.[21] In contrary, the CO_2/CH_4 solubility selectivity of [ImPE][Tf$_2$N] is very close to the value reported for [hmim][Tf$_2$N] in the literature (S_{CO2}/S_{CH4} =10 at 25°C).[11] Therefore, these results of ideal solubility selectivities show that a CO_2/N_2 gas separation process using the [ImPE][Tf$_2$N] IL will be the most effective at either ambient or lower temperatures and, as expected, the phosphonate-based ILs are not efficient to separate CO_2 from CH_4.

The first theory describing CO_2 solubility in ILs was based on the influence of anions, which were believed for longtime to play a primary role, whereas only minor influence was attributed to cations.[25] However, other works revealed that the CO_2 solubility also strongly depends on the cation alkyl chain length (*i.e., cation size*), for a given anion in imidazolium-based ILs.[11,17,26,27] In order to account for cation effect, several authors suggested that there is a free volume in the interionic space between the cation and the anion, which could play a significant role in dissolving CO_2.[28] To understand the evolution of CO_2 solubility results at 20°C and 40°C, we have estimated the free volume within the ILs, which is often considered as the underlying property d riving both gas solubility and selectivity.[29-31] From the work Shannon *et al.*[29], we have calculated the free volumes V_f (cm^3.mol^{-1}) of the phosphonate-based ILs in order to compare them with those of their conventional (non-phosphonated) ILs counterparts (Table 2). Calculation details are reported in *Supporting Information*. The phosphonate-based ILs contain ~40% higher free volume in comparison with their non-phoshonated analogues (*i.e.,* [bmim][Tf$_2$N] and [P$_3$mim][Tf$_2$N]). As an increase of the free volume should cause a decrease of CO_2 solubility[31], these results fit with the behavior of the phosphonate-based ILs at 40°C, but not

at 20°C. Hence, the sole free volume consideration cannot explain the results obtained for the solubility selectivity.

Table 2. Physical properties of the ionic liquids used in this study (at 22°C): ρ (ILs density (g.cm^{-3})), MM (molecular weight, g.mol^{-1}), V_m (molar volume, cm^3.mol^{-1}) and V_f (free volume, cm^3.mol^{-1}).

Ionic liquid	ρ (g.cm^{-3})	MM (g.mol^{-1})	V_m (cm^3.mol^{-1})/100	V_f (cm^3.mol^{-1})/100
[ImPE][Tf$_2$N]	1.48	541.43	3.66	0.54
[ImPEGPE][Tf$_2$N]	1.40	645.29	4.61	0.67
[bmim][Tf$_2$N]	1.43	419.37	2.93	0.38
[P$_3$mim][Tf$_2$N]	1.43	509.44	3.56	0.47

Some authors have suggested that the CO_2 solubility and associated selectivity could also depend on the strength of IL-gas interactions, the size of the cavities formed upon gas dissolution or on the conformational equilibria of the ions.[32] Indeed, the bulk structure of ILs is considered as nano-segregated, *i.e.,* anions and charged imidazolium rings organize into polar domains to form a 3-dimensional ionic network, while the alkyl chains of the cations (more than three carbon atoms) tend to segregate into non polar domains. When a gas dissolves in the IL, it induces conformational rearrangements of the ions which lead to the formation of cavities in both types of domains. In order to visualize the different domains of the ILs, Bara and co-workers[29,31] used the COSMOTherm software to generate the σ-surface of the ILs. This software generates a visual representation of the conformational equilibria for ILs. The individual charges and charge distribution in the molecules are optimized to minimize the system energy. Knowing the polarity distribution of the [C$_x$mim][Tf$_2$N] ILs, Horne *et al.*[31] were able to link the free volumes to both

the conformational equilibria of the ions and the CO_2 solubility in the corresponding ILs. To obtain the conformational equilibria of the phosphonate-based ILs used in the present study and visualize the polar/non polar domains, we have employed the quantum chemical DFT method which offers a good compromise between the required computational efforts and results reliability.[33] The structure of the phosphonate-based ILs was calculated at B3LYP level on the basis of the work of Buijs *et al.*[34]. After calculations of the optimum molecule geometry and energy, we were able to generate for each molecule the electrostatic potential (ESP) maps shown in **Figure 3** (See *Supporting Information* for calculation details). For each IL, the ESP map reveals the negative charges in red, the positive charges in blue, and the non-polar areas in green.
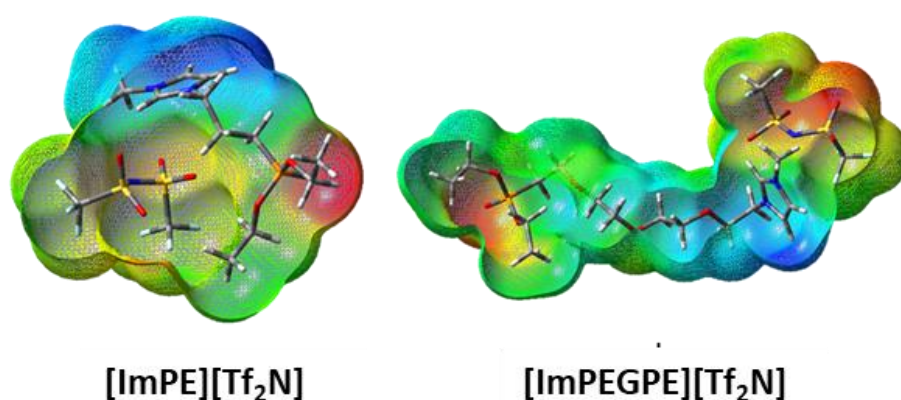

[ImPE][Tf$_2$N]   [ImPEGPE][Tf$_2$N]

Figure 3. Optimum molecule geometries and ESP maps of [ImPE][Tf$_2$N] and [ImPEGPE][Tf$_2$N] ILs synthesized in the present work. The calculated electrostatic potential maps are projected on the van der Waals surface (negative charges in red, positive charges in blue, and non-polar areas in green).

The ESP maps for the phosphonate-based ILs reveal two different equilibria conformations related to the two selected organic spacers *(i.e. propyl and glycol chains)* and negative ionic

domains linked to the coupling function. It must be noted that the size of cation in [ImPEGPE][Tf$_2$N] IL ($\approx$ 20 Å) is significantly higher than in [ImPE][Tf$_2$N] IL ($\approx$ 12 Å). Similar to [P$_3$mim][Tf$_2$N], the ethylene glycol groups of the [ImPEGPE][Tf$_2$N] phosphonate-based IL creates additional ionic domains in the final equilibria conformation. As the number of ionic domains is more important in the [ImPEGPE][Tf$_2$N] ILs, the quantity of cavities created under gas dissolution is potentially higher than in [ImPE][Tf$_2$N]. Indeed, the difference of N$_2$ solubility between these two phosphonate-based ILs could be explained by both the N$_2$ dissolution dominated by the partial molar Gibbs free energy of cavity formation and bigger size of the cation.[32] Even if more detailed simulations are needed to characterize and quantify both the size distribution and the nature of cavities, these first results reveal the impact of the organic spacer on the IL molecule conformation and the location of the apolar and ionic domains. In addition, studies on the IL-gas interactions should be considered to confirm the absence of any chemisorption phenomena between CO$_2$ and the phosphonate-based ILs. Finally, it may be strongly relevant, although highly tricky, to investigate how the grafting reactions of these ILs on a ceramic support will modify the charge distribution and conformation of the molecules.

3.2. Viscosity measurements and CO$_2$ diffusion coefficient

As reported by Scovazzo[16] gas selectivity of SILMs is assumed to be dominated by the solubility selectivity. However, two parameters can influence the gas diffusion coefficient in SILMs: the IL viscosity and its molar volume. Scovazzo et al.[35-37] studied gas diffusivity in conventional ILs and developed a diffusivity model to predict the permeability of synthesized SILMs. According to Morgan et al.[35], the CO$_2$ diffusivity, $D_{CO2,bulk}$ (cm².s⁻¹), in bulk ILs can be estimated by using the following equation:

$$D_{i,bulk} = 2.66 \times 10^{-3} . \frac{1}{\mu_{IL}^{0.66}.V_{CO2}^{1.04}} \tag{3}$$

with μ_{IL} *(mPa.s),* the IL viscosity and V_{CO2} *(cm³.mol⁻¹),* the molar volume of CO_2.

The evolution of viscosity values vs. temperature for the phosphonate-based ILs is shown in **Figure 4** and compared with the trend observed for conventional IL (*e.g., [emim][Tf₂N], [bmim][Tf₂N]*). The [ImPE][Tf₂N] is more viscous than the [ImPEGPE][Tf₂N] IL and both phosphonate-based ILs are at least 9 times more viscous at 20°C than conventional ILs.
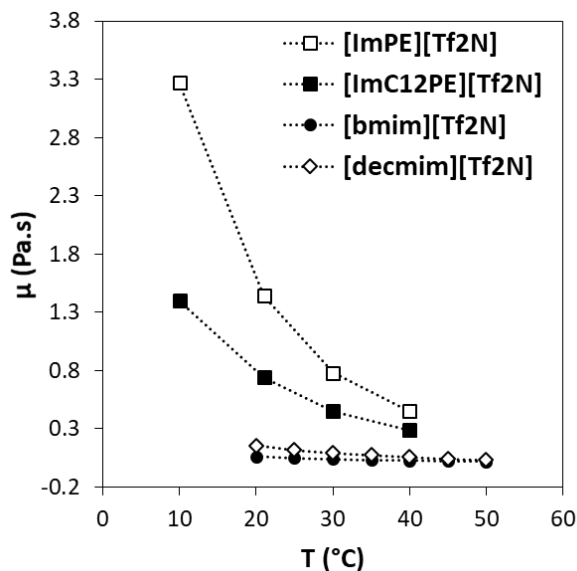

Figure 4. Evolution of the viscosity of the phosphonate-based ILs ([ImPEGPE][Tf₂N], [ImPE][Tf₂N]) vs. temperature, and comparison with conventional ILs ([bmim][Tf₂N], [decmim][Tf₂N]).

By using both these viscosity values and Eq. 3, it was possible to estimate the CO_2 diffusion coefficient at 20°C in the phosphonate-based ILs (**Table 3**), considering that gas transport through IL-based membranes is governed by the solution-diffusion mechanism. The CO_2 permeability values for the membranes made with physisorbed ILs were quite low. In the case of GILMs, the IL is immobilized in the support and thus its viscosity is not expected to play an important role in comparison with conventional SILMs containing physisorbed ILs. Because of

21

that, the gas diffusion coefficients and gas permeability values are expected to be different for these two types of membranes.

Table 3. Viscosity (**μ**), CO_2 diffusion coefficient (**D_{CO2}**), CO_2 solubility coefficient (**S_{CO2}**) and estimated CO_2 permeability (**P^*_{CO2}**) for phosphonate-based ILs at 20°C. Viscosity, CO_2 diffusion coefficient, CO_2 solubility coefficient and estimated CO_2 permeability of the phosphonate-based ILs at 20°C.

ILs	μ (Pa.s) at 20°C	D_{CO2} x 10^6 ($cm^2.s^{-1}$)	S_{CO2} xs 10^{-2} (cm^3 (STP)/(cm^3.cmHg) at 20°C	P^*_{CO2} (Barrer)
[ImPE][Tf$_2$N]	1.44	0.9	0.035	30.1
[ImPEGPE][Tf$_2$N]	0.74	1.3	0.035	46.7

3.3. Grafted Ionic Liquid Membranes (GILMs)

Grafted Ionic Liquid Membranes have been prepared by applying the optimized grafting protocol of phosphonate-based ILs on the γ-Al_2O_3 top-layer of commercial alumina discs. In order to compare the GILMs prepared in this work with the SILMs described in the literature, ceramic-based SILMs were synthetized with 1-butyl-3-methylimidazolium bis(trifluoromethanesulfonimide) ([bmim][Tf$_2$N]), using the same alumina disc as for the GILMs. The morphology, composition, and thickness of the three as-prepared membranes have been analyzed and compared, together with their performance (permeance and selectivity) for gas transport.

3.3.1. Physico-chemical characterization of the membrane samples

The preparation of GILMs was conducted by reacting the γ-Al_2O_3 top-layer with a phosphonate-based IL solution at 130°C, using the optimum reaction conditions determined in our previous study.10 The quantity of phosphonate-based ILs and grafting reaction time (**Table 1**) used for

the synthesis corresponds to a maximum quantity of grafted species on the γ-Al_2O_3 powder.[10] After the grafting treatment, the GILMs were washed by immersion in an ethanol-water solution (60/40 vol.%) during 5 min to remove the excess of IL and then dried at 70°C. The [bmim][Tf_2N]-SILM membrane was prepared according to a procedure reported in the literature.6

Scanning Electron Microscopy (SEM) observations were used to compare the pristine alumina support and the membrane morphology, location of the IL and homogeneity of [bmim][Tf_2N]-SILM, GILM(1), GILM(2)). Membrane cross-sections are shown in **Figure 5** with zooms of different areas of the membranes. The pristine alumina support is shown in **Figure 5** (A1, A2, and A3), the [bmim][Tf_2N]-SILM in (B1, B2 and B3), the [ImPE][Tf_2N]-GILM(2) in (C1, C2, and C3) and the [ImPEGPE][Tf_2N]-GILM(2) in (D1, D2, and D3). **Figure 5**. A1 shows the pristine γ-Al_2O_3 top-layer ($\varnothing_{pores}$= 5 nm); A2 shows the top-layer and two underlayers ($\varnothing_{pores}$= 100 and 800 nm) and A3 shows the external support layer ($\varnothing_{pores}$= 3 μm). In each SEM micrograph, the pores and alumina grains forming the membrane are clearly visible. In the case of the [bmim][Tf_2N]-SILM, SEM observations were carried out after the gas permeation tests. The **Figure 5** (B1 and B2) reveal the homogeneous impregnation of the IL along the support cross-section in both the γ-Al_2O_3 top-layer and support underlayers. On the external support layer (B3), only small amount of physisorbed IL can be observed in between the alumina grains. From SEM analysis, we can estimate the membrane composite layer thickness at ~33 μm. When comparing the micrographs of [bmim][Tf_2N]-SILM to those of [ImPE][Tf_2N]-GILM(1) in **Figure 5** (C1, C2, and C3), the alumina grains (γ-Al_2O_3 and α-Al_2O_3) of the top-layer and internal layers respectively, are more visible in figures C1 and C2. The surface does not appear smooth like in the previous case but rather rough. The grains of the external layer seem to be

23

coated with the [ImPE][Tf$_2$N] IL. The thickness of the hybrid layer was estimated at ~20 μm also for [ImPE][Tf$_2$N]-GILM(1). Finally, the micrographs corresponding to [ImPEGPE][Tf$_2$N]-GILM(2) (**Figure 5**. D1, D2, and D3) were very similar to those of [bmim][Tf$_2$N]-SILM except that no IL was detected in the external layer (D3). From the SEM observations of the membranes cross-section it can be concluded that the phosphonate-based ionic liquid is present not only in the gamma alumina top-layer but also in the α-alumina under-layer (Tab S1).
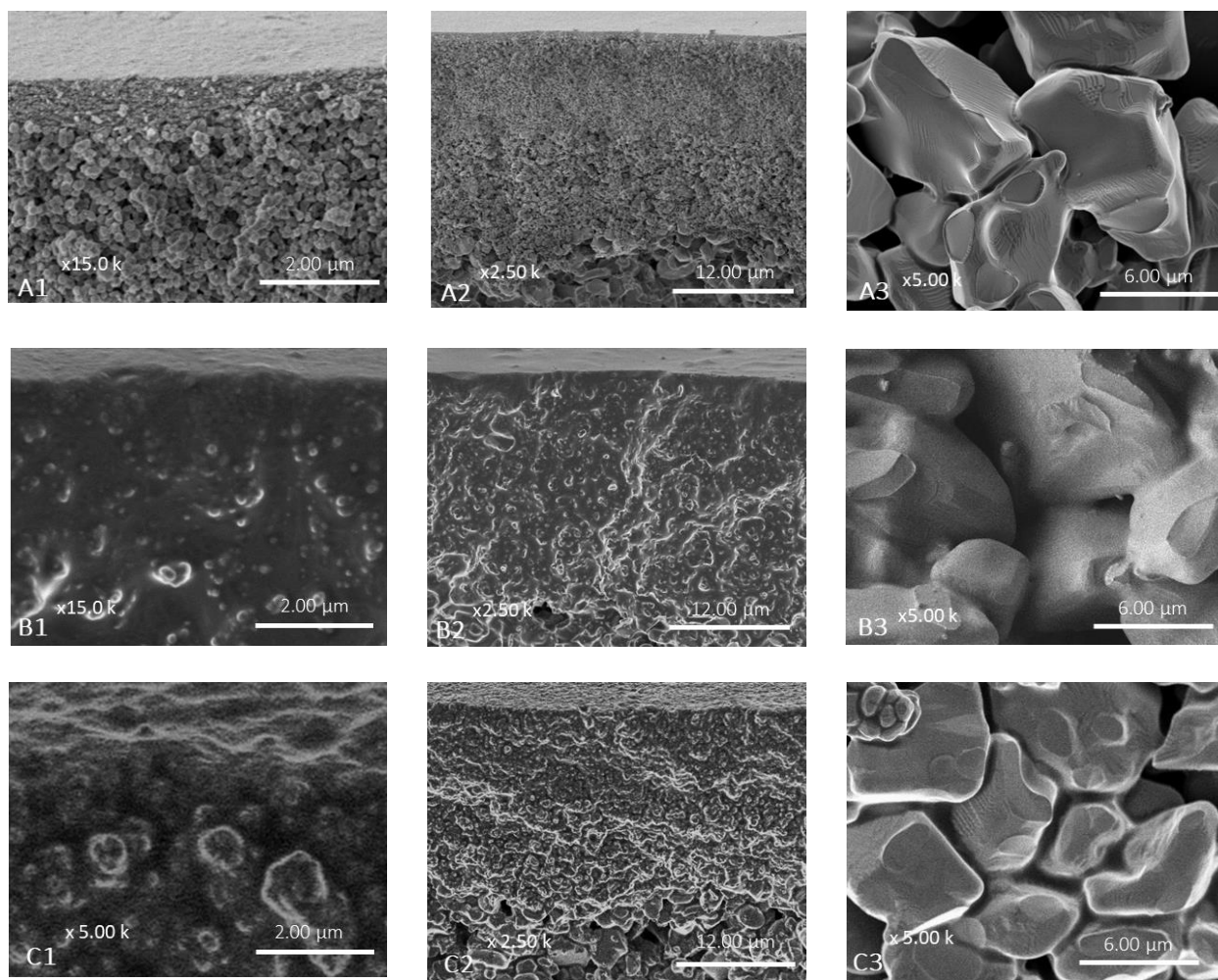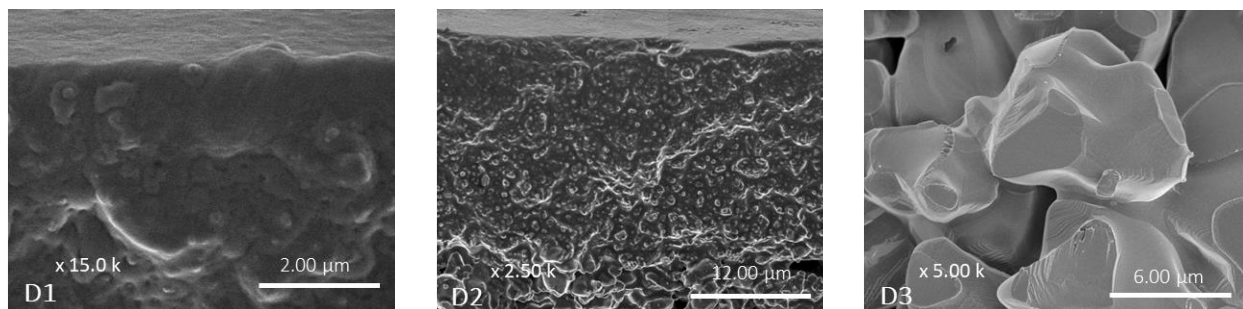
Figure 5. SEM pictures showing the cross-sections of the alumina support with γ-Al$_2$O$_3$ top-layer before and after IL impregnation/grafting: A) pristine support, B) [bmim][Tf$_2$N]-SILM, C) [ImPE][Tf$_2$N]-GILM(1), D) [ImPEGPE][Tf$_2$N]-GILM(2). The numbers 1, 2 and 3 refer to different areas of the membranes: 1. γ-Al$_2$O$_3$ top-layer (Ø$_{pores}$= 5 nm) and first underlayer (Ø$_{pores}$= 100 nm), 2. γ-Al$_2$O$_3$ top-layer and two underlayers (Ø$_{pores}$= 100 and 800 nm), and 3. external support layer (Ø$_{pores}$ = 3 μm).

In order to investigate the grafting of phosphonate-based ILs in the GILMs, a FTIR study was conducted directly on the γ-Al$_2$O$_3$ top-layer surface in ATR mode for both the GILM(1) and GILM(2) samples (**Figure 6**). The spectra of the pure [ImPE][Tf$_2$N] and [ImPEGPE][Tf$_2$N] phosphonate-based ILs are dominated by absorption bands related to the Tf$_2$N$^-$ anion, asymmetric and symmetric -SO$_2$ stretching vibrations at respectively 1327-1346 and 1132 cm^{-1}, -CF$_3$ stretching vibration at 1224 cm^{-1} and -SNS stretching vibration at 1061 cm^{-1}.[38] Based on DFT calculations, we were able to estimate the different vibration modes and associated wavenumbers of the coupling functions (Figure S4). It was then possible to identify several vibrations such as the P=O stretching vibration at 1266 cm^{-1} for [ImPE][Tf$_2$N] and 1236 cm^{-1} for [ImPEGPE][Tf$_2$N], the asymmetric and symmetric P−O−C stretching vibrations at 960 and 1050 cm^{-1}, and the C-H and -CH$_2$ stretching vibration at 1017 cm^{-1} and 1195 cm^{-1}, respectively.[15,39] In the FTIR spectra of the GILM(1) and GILM(2) samples, we can also notice

the predominance of the Tf$_2$N$^-$ bands which confirmed that the structure of the grafted imidazolium has been maintained as expected from EDX measurements (**Table 1**, *e.g.,* ratio P:S = 1:1.5 (expected 1:2)). The presence of the cationic part is denoted by a strong vibration band at 1171 cm^{-1}, characteristic of the =CH and –CH$_2$– deformation vibrations of both the imidazolium ring and the organic spacers. The grafting of the coupling function on the alumina surface is clearly indicated by the reduction of the bands related to the phosphoryl (P=O) stretching vibration near 1266 and 1236 cm^{-1}, indicating the coordination of the P=O bonds to alumina Lewis acid sites. Moreover, the grafting is further confirmed by the presence of residual bands connected to the –POEt groups in the region 950-1050 cm^{-1}, suggesting that most of them have reacted with Al-OH surface groups. Finally, it is important to point out the presence of the strong P-O-Al stretching band at 1065 cm^{-1} in both GILMs, thus confirming the presence of grafted ILs on the γ-Al$_2$O$_3$ porous ceramic layer.[10,15]
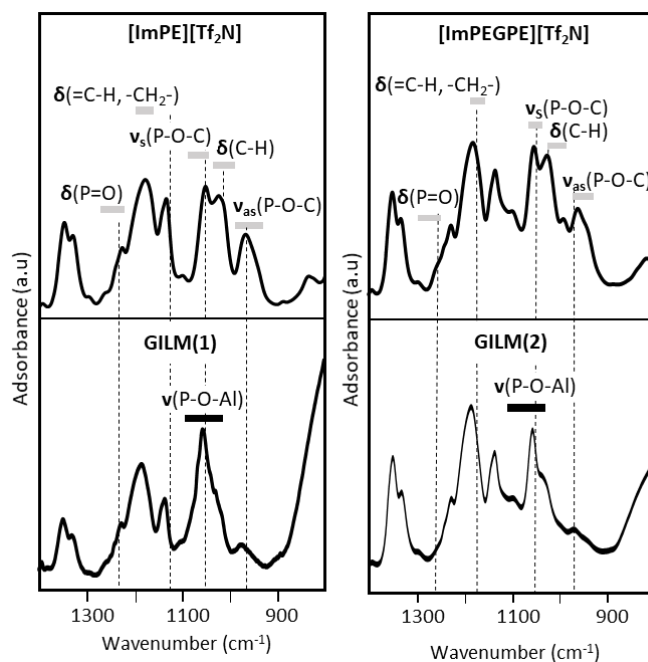

Figure 6. Experimental FTIR spectra of the phosphonate-based ILs and the corresponding grafted IL membranes GILM(1) and GILM(2).

In our previous work[10], FTIR and ^{31}P Solid-State NMR were employed to study the influence of the grafting reaction conditions on the bonding modes of phosphonate-based ILs, grafted on γ-Al$_2$O$_3$ powders. However, conventional SS NMR is not directly applicable to grafted IL membranes because of the relatively low amount of grafted species per unit volume of the ceramic sample (*considering that there is only 0.2% of γ-Al$_2$O$_3$ in the whole volume of α-Al$_2$O$_3$ ceramic disc*). Recently, ^{1}H High Resolution-MAS NMR at 10 kHz was used to investigate macroporous alumina membranes (pore size ~200 nm) containing N-methyl-N-(n-butyl)pyrrolidinium bis(trifluoromethanesufonyl)imide [MBPyrr][Tf$_2$N] IL physisorbed in their porous network.[40] The authors were able to identify the ^{1}H nuclei affected by IL/oxide surface interactions. Moreover, by using the 2D ^{1}H HR-MAS NOESY NMR experiments, the authors also showed that correlation experiments could demonstrate the decrease of local motions, the presence of different conformations, and the appearance of new chemical environments for the adsorbed IL. HR-MAS NMR experiments are known to provide significant spectra resolution improvements even at moderate spinning rates, in comparison with basic solid-state NMR experiments, due to motional narrowing of the NMR linewidth allowed by the presence of the solvent. The HR-MAS method is a perfect tool for samples which are in the liquid/solid classification.[40] In the present work, HR-MAS spectroscopy was used to enhance the resolution of ^{1}H, ^{19}F and ^{31}P NMR spectra (Figure 6) of the GILM(1) sample thanks to the degrees of freedom agreed to the motion of the organic part in the solvent at the surface of the ceramic. By comparison with the ^{1}H liquid NMR spectra of the neat IL (**Figure 7**.I.a), it was possible to observe that the ^{1}H HR-MAS NMR spectra of GILM(1) (**Figure 7**.I.b), present protons from the imidazolium ring (H$_2$, H$_3$, and H$_1$) with various singlet signals (see **Figure S5** for a zoom) and negligible changes in their chemical shift (Δδ < 0.1 ppm). The ^{1}H signals related to the organic

spacer (H_5, H_6, and H_7) are at the expected position and present asymmetrical shapes. The ^1H nuclei representing the coupling functions (H_8 and H_9) were also visible at 3.95 and 1.71 ppm. These results suggest either a part of the coupling functions is involved in the grafting, or the presence of physisorbed IL (trapped by electrostatic interactions). One additional ^1H signal was observed (compared to the neat IL) at 3.59 ppm, which is attributed (from the ^1H-^{13}C gHSQC experiment, Figure S6) to water species adsorbed on the γ-Al_2O_3 surface. Concerning the Tf_2N^- anion in the grafted membrane, the ^{19}F NMR liquid spectrum of pure IL [ImPE][Tf_2N] displays a sharp peak corresponding to the –CF_3 functions at -78.7 ppm (**Figure 7**.II.a), while the ^{19}F HR-MAS NMR spectra of the grafted membrane GILM(1) (**Figure 7**.II.b) shows a broad signal centered at a similar position of -78.8 ppm. The sharpening line in the ^{19}F liquid spectra of the IL was due to stronger "motional narrowing" in liquid (caused by Brownian motion) than in the confined areas of the hybrid materials. The broader signal in the grafted samples can be explained by the cation immobilisation on the γ-Al_2O_3 surface, thus reflecting the difference between immobilized/grafted IL and pure liquid phase. No other signal was detected, thus confirming that Tf_2N^- anions were preserved during the grafting process, as suggested also by FTIR spectroscopy. ^{31}P HR-MAS NMR is an essential tool both to highlight the presence of phosphorus atoms in the hybrid materials and to distinguish between grafted and physisorbed species.[10] The ^{31}P HR-MAS NMR spectrum of the GILM(1) sample is shown in **Figure 7**.III.b. The good resolution of these spectra allows evidencing the presence of physisorbed species identified by a sharp signal at 30.32 ppm. Additionally, a broader signal centered at 23.74 ppm can be observed, which is associated to the grafted species in dominating tridentate bonding mode configuration (figure S7).[10] The integration of the two dominant signals revealed that the proportion percentage of physi- and chemisorbed in the GILM was respectively 56.8 and 43.2%.
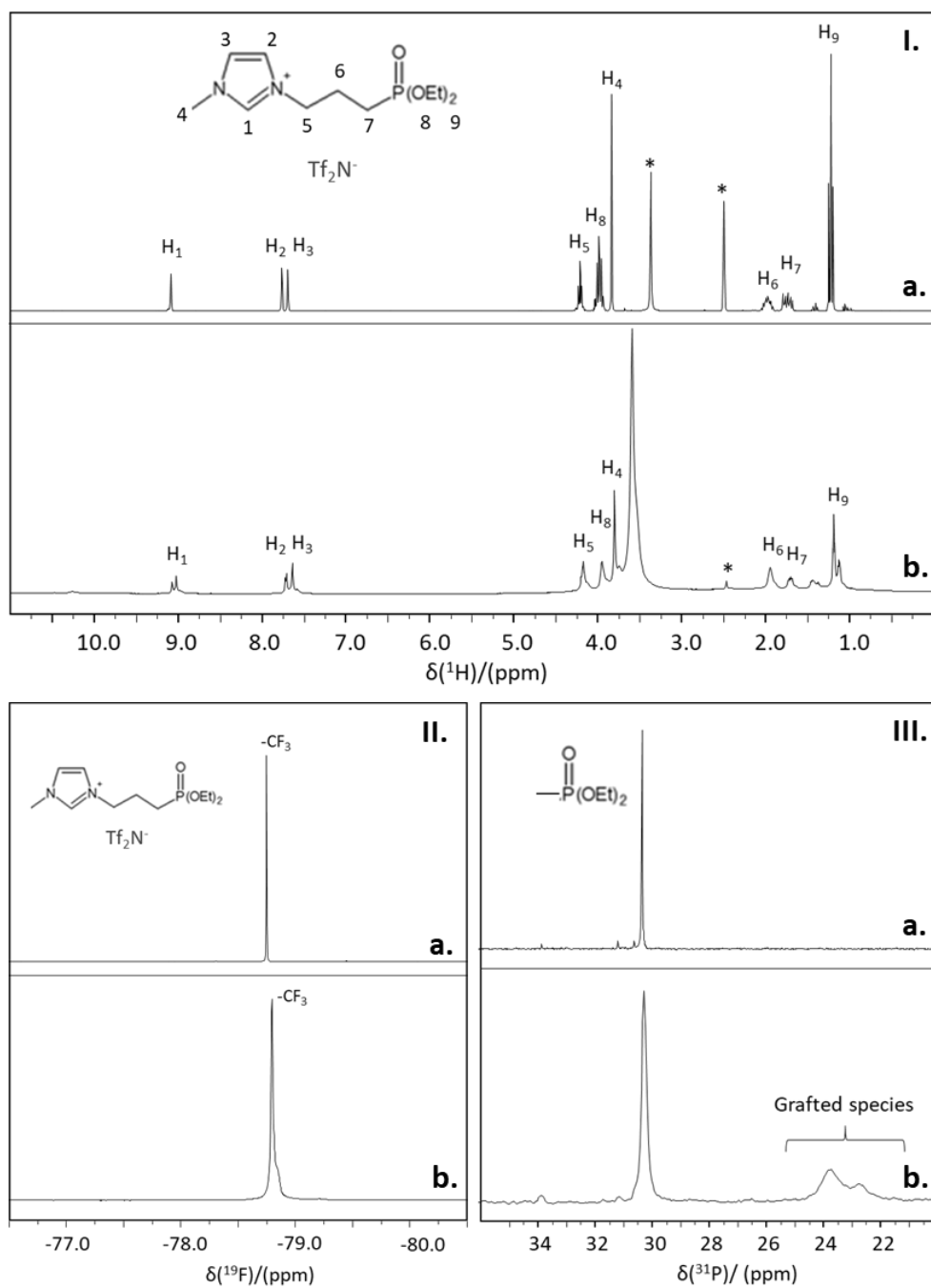
Figure 7. ^1H (I.), ^{19}F (II.) and ^{31}P (III.) NMR spectra in DMSO of a. pure IL [ImPE][Tf$_2$N] (liquid NMR measurements) and b. [ImPE][Tf$_2$N] grafted membrane GILM(1) (HR-MAS NMR measurements).

The penetration/grafting depth of the ILs into the γ-Al$_2$O$_3$ porous support (hybrid membrane thickness) has been also estimated from EDX analyses of the phosphorus and sulfur contents along the membrane cross-section (from the γ-Al$_2$O$_3$ top-layer to the support external layer) (**Table 4**). This approach was used by Drobek *et al.*[41] to study the infiltration depth of fluorinated oligomers in zeolite membranes. In the present work, phosphorus and sulfur were analyzed as tracers of the coupling function of the cation and anion, respectively. Results of thickness evaluation for GILM(1), GILM(2) and [bmim][Tf$_2$N]-SILM are reported in **Table 4** and **Figure 8**. As shown in **Table 4**, the thickness values **(T)** derived from both SEM micrographs and EDX analysis are very close. The IL penetration depth in both [bmim][Tf$_2$N]-SILM and GILM(2) are estimated at ~30 µm. The hybrid membrane thickness for GILM(1) was determined ~23 µm from the SEM observations, and ~25 µm from EDX analysis. Hence, considering similar results obtained by SEM observations and EDX analysis, in this work we used the membrane thicknesses determined by SEM (T$_{\textbf{SEM}}$) for [bmim][Tf$_2$N]-SILM and both GILM(1) and GILM(2).
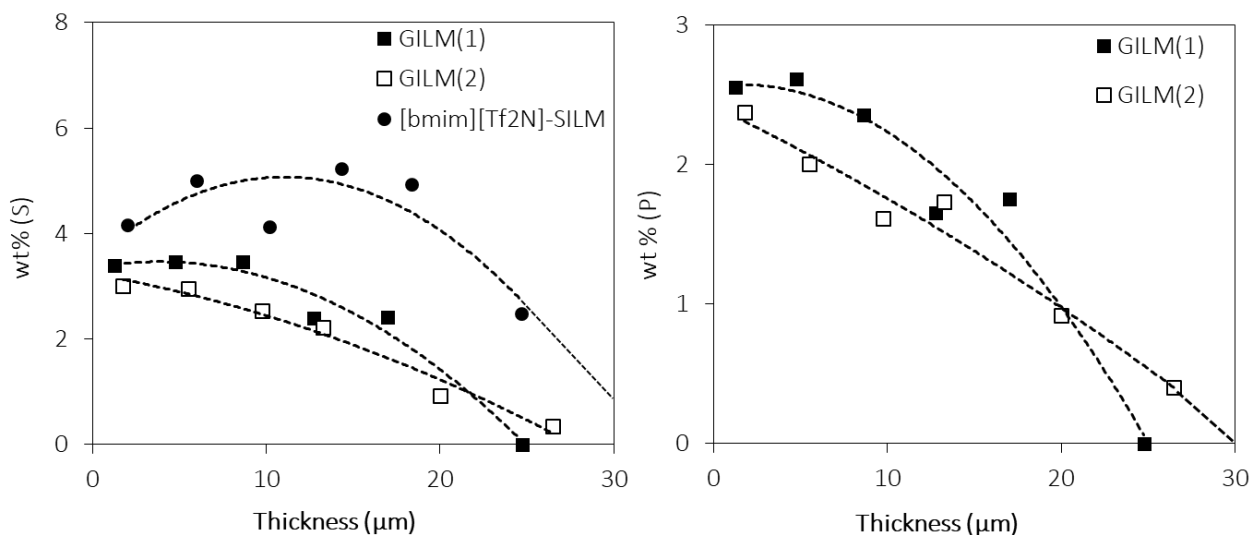
Figure 8. Evolution of phosphorus (left side) and sulfur (right side) concentrations (wt% by EDX analysis) along the membrane cross-section (μm) for GILM(1), GILM(2) and [bmim][Tf$_2$N]-SILM.

3.3.1. Single gas permeation measurements

The **Table 4** compares the single gas CO_2 permeances (Π_{CO2}) and ideal CO_2/N_2 selectivities (α*) measured at 23°C for the 3 IL-based membranes and for the pristine γ-Al$_2$O$_3$ mesoporous membrane. It should be noted that all the hybrid membranes were found to be N$_2$-tight or at least below the system permeation detection limit, ($< 1 \times 10^{-11}$ mol.m^{-2}.s^{-1}.Pa^{-2}). This finding thus proves that the hybrid membranes are defect-free and continuous, with the IL fully occupying the pores of the γ-Al$_2$O$_3$ top-layer.

It should be noted that the values of single gas permeances through the IL-membranes developed in this work were measured in a dead-end configuration, *i.e.,* conditions favoring gas transport through membrane defects, if any. Many results reported in the literature are obtained with a Wicke-Kallenbach configuration (steady state diffusion cell)[6], which limits the contribution of membrane defects to gas transport and thus yields high (and sometimes huge) gas selectivities which are hardly reproducible in industrial systems. **Figure 9** compares the CO_2/N_2 ideal selectivity vs. CO_2 single gas permeability at ~25°C for series of IL-based membranes prepared in this work, with data from the open literature (*e.g., cross-linked PIL/IL ion-gels membranes, PIL membranes, ceramic and polymeric SILMs*). For the sake of a relevant comparison, only IL-based membranes with the same cationic core (imidazolium-based IL) and predominantly [Tf$_2$N]$^-$ anion were considered in the Robeson plot.

Table 4. Comparison of single CO_2 permeance (Π_{CO2}) and ideal CO_2/N_2 selectivity (α^*) for three IL-based membranes, [bmim][Tf$_2$N]-SILM, GILM(1) and GILM(2) and for the pristine γ-Al$_2$O$_3$ mesoporous membrane. IL penetration depth (hybrid membrane thickness) (T) were obtained from SEM pictures, and confirmed by EDX analysis. Permeances were measured at 23°C with a feed pressure of 3.5 bar. For all IL-based membranes Π_{N2} was below the system detection limit (*i.e.,* $< 1 \times 10^{-11}$ mol.m^{-2}.s^{-1}.Pa^{-2}).

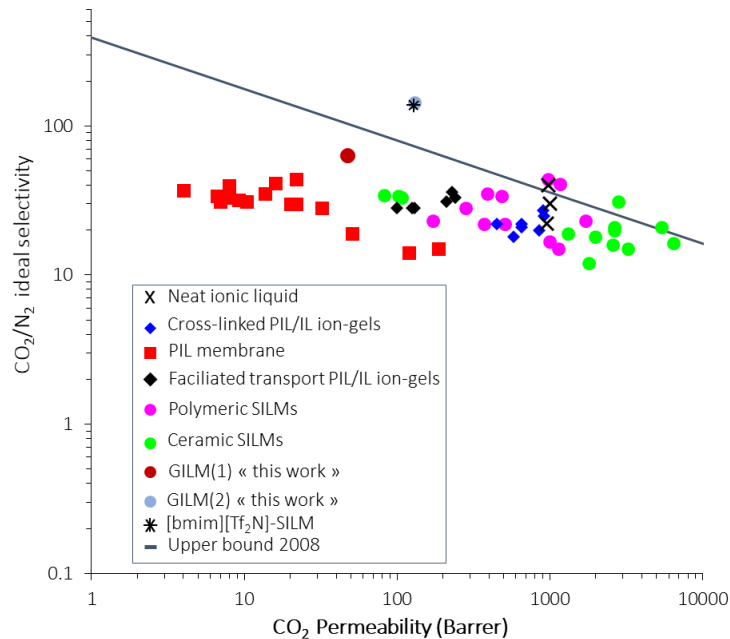| Sample	Virgin γ-Al$_2$O$_3$	[bmim][Tf$_2$N]-SILM	GILM(1)	GILM(2)
Π_{CO2} (mol.m^{-2}.s^{-1}.Pa^{-1})	3.30×10^{-6}	1.43×10^{-9}	6.2×10^{-10}	1.32×10^{-9}
Π_{CO2} (GPU)	9859	4.3 ± 0.5	1.8 ± 0.1	3.9 ± 1.0
T_{SEM} (μm)	-	31	23	30
T_{EDX} (μm)	-	28	25	30 ± 2
P^*_{CO2} (Barrer)	-	132.7 ± 5.3	47.4 ± 2.7	129.7 ± 21.2
α^* (CO_2/N_2)	0.9	143.3 ± 4.8	63.5 ± 3.7	144.1 ± 23.5

Figure 9. Robeson plot showing the CO_2/N_2 ideal selectivity performance vs. CO_2 single gas permeability of the GILMs prepared in this work, in comparison with IL-based membranes from the literature. *(All data points correspond to measurements at room temperature (20-30°C) with a feed pressure between 0.5 and 3.5 bar for membranes composed of ILs with imidazolium-based cationic core and predominantly [Tf_2N]⁻ anion).*

It must be noted that a displacement of the [bmim][Tf$_2$N] IL under high pressure is possible. Hence, the membrane weight has to be measured before and after the gas permeation tests. A weight loss of 4% was typically measured by Albo *et al.*[42] after 25h experiment at 2 bar and 25°C for a system [emim][ac]/porous Al_2O_3/TiO_2 membranes. In fact, as reported by Gan *et al.*[43], the utilization of "nanoporous" membrane supports, with sufficiently small pore diameters, can improve the stability of immobilized ILs up to 7 bar transmembrane pressure. Thus, having measured a negligible weight loss (less than 4%) for the prepared GILMs at 3.5 bar, we can assume that the blown-out pressure is higher than 3.5 bar. The small mesopores and non-negligible tortuosity of the γ-Al_2O_3 membrane contributes to an efficient confinement of the IL within the pores. The CO_2 permeability of [bmim][Tf$_2$N]-SILM is remarkably low in comparison with published results for SILMs prepared by impregnation of [bmim][Tf$_2$N] in other ceramic supports. For example, Close *et al.*[6], reported a CO_2 permeability of 2582 Barrer with a CO_2/N_2 ideal selectivity of 16 for a SILM prepared by impregnation of [bmim][Tf$_2$N] in alumina Anodisc support with tortuosity ~1 (parallel cylindrical pores). In the present work the tortuosity of the γ-Al_2O_3 top-layer is much higher than 1 (around 5), thus favoring higher IL/gas contact time and thus yielding higher ideal CO_2/N_2 selectivity (typically > 143 instead of ~16 for the Anodisc support).[6] The same phenomenon was observed by Labropoulos *et al.*[44], when impregnating a micropororous silica top-layer ($\varnothing_{pore}$ ~ 1 nm) with either [emim][TCM] or [bmim][TCM] ILs.

The authors observed high selectivities of CO_2/N_2 gas pair but low CO_2 permeability for all the prepared SILMs.[44] The confinement of the IL in the micropores was invoked to generate strong increase of its viscosity and thus an expected decrease of CO_2 permeability. In addition, the authors suggested that the confinement of [bmim][TCM] IL induces specific orientation, favoring CO_2 transport through a hopping mechanism from anion to anion, while the [emim][TCM] IL was exposed to a liquid/solid transition affecting the CO_2 diffusion. This assumption was demonstrated elsewhere[45], by comparing series of ceramic-based SILMs derived from the [C$_x$mim][TCM] ILs impregnated in either microporous (silica with $Ø_{pore} \sim 1$ nm) or mesoporous (γ-Al$_2$O$_3$ with $Ø_{pore} \sim 5$ or 10 nm) top-layers. Thermal analysis of these SILMs revealed a drastic liquid-to-solid transition upon confinement of the ILs in micropores with sizes ~ 1 nm. The authors concluded that the IL was under different physical states depending on the pore sizes, thus yielding significant variation in the gas transport properties and CO_2 permeability. The results we obtained for the [bmim][Tf$_2$N]-SILM fit those reported by Labropoulos and co-workers[44,45] and could be associated to confinement effects.

The grafted ionic liquid membranes, GILM(1) and GILM(2), also yield relatively high CO_2/N_2 ideal selectivities (> 64 and >144, respectively), similar to those measured for the [bmim][Tf$_2$N]-SILM in which the IL is simply physisorbed in the pores. The CO_2 permeability is also in the same range, with values of 47 Barrer for GILM(1) and 130 Barrer for GILM(2). These CO_2 permeability values fit those published by Vangeli *et al.*[6], for microporous ceramic membranes grafted with alkoxysilane imidazolium ILs. The chemical grafting of the [smmim][PF$_6$] IL was investigated by EDX analysis, and was argued to explain the observed gain of stability (CO_2 permeability) obtained during 3 sequential heating/cooling cycles up to 250°C, and 5 bar trans-membrane pressure. The highest CO_2 permeability measured at 30°C was

~226 Barrer for the modified microporous silica membrane ($\emptyset_{pore} \sim 1\ nm$). This permeability is close to the values obtained in the present work for both GILM(2) and [bmim][Tf$_2$N]-SILM. Permeation measurements performed at higher temperatures (50 and 100°C) did not reveal any significant influence of temperature on the CO_2 permeability (127±9 Barrer) while the N_2 permeability was increased by a factor x12 (from 1 to 12 Barrer). The evolution of the CO_2/N_2 ideal selectivity vs. temperature is shown in **Figure 10**. At 100°C the CO_2/N_2 ideal selectivity was found to drop down to 15 ± 6, although a value of 144 ± 24 was measured at 30°C. According to **Figure 10**, these results do position the GILM(2) performance at 100°C in the region of the PIL membranes which are considered as rigid structures. This conclusion might be surprising when considering the outcomes of CO_2 and N_2 solubility measurements discussed in section 3.1. However, as evoked previously, once the IL is grafted on the ceramsic support the ILs properties characteristic for the bulk are lost. As communicated in the physico-chemical characterization part of the manuscript, approximately 50% of the IL is grafted onto a ceramic membrane support, while the rest is just physisorbed. The trends observed in gas permeation experiments are thus a consequence of the contribution of both physi- and chemisorbed ILs. Hence, for the future works, following the initial steps towards the development of GILMs studied in this work it will be strongly relevant to investigate how the partial grafting reactions of these ILs on a ceramic support modify both gas diffusion (*depending on the viscosity of the physisorbed ILs trapped by weak interactions within the grafted ILs*) and solubility coefficients.
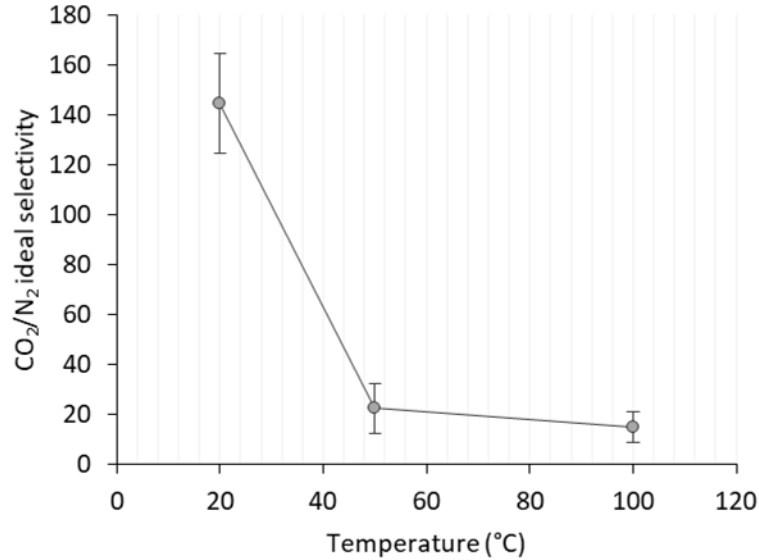
Figure 10. Evolution of the CO_2/N_2 ideal selectivity in function of the temperature for the membrane GILM(2).

Such investigation will be of major impact for increasing the CO_2 permeability which is currently limited to ~5 GPU for all the GILMs developed in this work. According to Merkel *et al.*[47], the membranes designed to treat flue gas usually operate in a pressure-ratio-limited regime and CO_2 permeances of ~1000 GPU are typically required to limit the membrane area and associated capital cost. High selectivity only increases gas purity and impacts on both power requirements and operating costs, this is why a CO_2/N_2 selectivity of ~30 is often enough. Thus, application of GILMs to flue gas treatment will be possible only if higher CO_2 permeance can be reached. This will be the objective of our future work by decreasing the membrane thickness from 30 to 1 µm *(e.g. by using thinner γ-alumina membrane supports)*. Applying slightly higher temperature for activating CO_2 transport will be also attempted, as the GILMs synthesized at 130°C should withstand operating temperature up to 110-120°C. In addition, as far as nanoconfined IL-based SILMs have been shown to provide an increase of CO_2 permeability with stable CO_2 selectivity at higher temperatures (i.e., 250°C), attractive performance is expected for

36

the GILMs for the separation of gas mixtures upon long term operation.[6,44,45] This hypothesis will need to be demonstrated by comparing single gas permeation and gas mixture separation through both SILM and GILMs for long period of time, at high temperature and/or high pressure.

4. CONCLUSION

The present work is focused on a fundamental step towards the development of new Grafted Ionic Liquid Membranes (GILMs) in which selected phosphonate-based ILs are confined within the pores of a mesoporous γ-Al_2O_3 ceramic membrane by chemical grafting.

As a first step in the conception of GILMs we have reported on CO_2, N_2, and CH_4 solubility performance of phosphonate-based ILs, *i.e.* [ImPE][Tf_2N] and [ImPEGPE][Tf_2N]. The CO_2 solubility values were found to be lower than those of their conventional analogues, with remarkably high CO_2/N_2 ideal solubility selectivity for [ImPE][Tf_2N] at 20°C. The computational study of these ILs revealed the influence of both the coupling function and the organic spacer on the polarity and equilibrium conformation. The difference of both conformation and polar domains between the two ILs could possibly explain the differences of both N_2 solubility and CO_2/N_2 selectivity.

In the second part of this study, we investigated the GILMs prepared on γ-Al_2O_3 ceramic supports by applying the synthesis protocol developed in our previous work.[10] Special attention has been devoted to an assessment of the best grafting conditions for the selected ILs, yielding maximum grafting density and avoiding any potential γ-Al_2O_3 support dissolution. The efficiency of the grafting reaction was clearly demonstrated by FTIR and HR-MAS NMR, while the morphology and physico-chemical characteristics of the membranes were investigated by SEM and EDX measurements. In spite of their low CO_2 permeability (~130 Barrer) the best

membranes prepared with the [ImPEGPE][Tf$_2$N] IL were found to exhibit high CO_2/N_2 ideal selectivity ($\sim$144) outperforming the classical Robeson upper bound limit.[46] As far as nanoconfined IL-based SILMs have been shown to provide an increase of CO_2 permeability with stable CO_2 selectivity at higher temperatures, attractive performance is expected for the separation of gas mixtures with the GILMs upon long term operation. This study will be the subject of our future investigations focusing in more details on the gas permeation and separation measurements for long period of time, at high temperatures and/or high pressures. It can be concluded that using a multidisciplinary approach combining organic chemistry, chemical engineering and materials science, a number of original results emerge from this research work targeting both the preparation of new ionic liquids and novel membrane systems as first steps towards the development of stable Grafted Ionic Liquid Membranes for the selective transport of CO_2.

   Furthermore, the prospects of this exploratory research work are expected to be much wider than only acid gas separations, especially when considering the extension of the grafting strategy to other support/IL systems. Indeed, phosphonate-based ILs could be grafted on various types of porous ceramic oxide supports (*e.g., TiO$_2$, ZrO$_2$, ZnO, HDL compounds, zeolites...*) and several hybrid porous supports could be considered too, such as MOFs. Taking advantage of the specific properties of both the selected support and the IL species, the developed IL-grafted membranes could be used to implement the separation of various mixtures (*e.g., gases, alcohols, organic acids, esters and aromatic hydrocarbons*), to fabricate advanced electrochemical devices (*e.g., lithium batteries, fuel cells and solar cells*), and to facilitate catalytic reactions.[3] Phosphonate-IL grafted layers could also serve as efficient antimicrobial, hydrophilic-hydrophobic surfaces for a variety of membrane applications.

ASSOCIATED CONTENT

Supporting Information: The description of the used γ-Al$_2$O$_3$ porous ceramic support, ionic liquids volumetric mass density measurements, details on the gas solubility measurements, schematic representation of the single gas permeation installation, and detail information on the molecular modeling. In addition, the document contains the FTIR spectra of the ILs in ATR mode and DFT calculated spectra, zoom of the ^{1}H and ^{31}P HR-MAS NMR spectra of GILM(1), results of the ^{1}H-^{13}C gHSQC HR-MAS NMR experiment of GILM(1). This material is available free of charge via the Internet at http://pubs.acs.org.

AUTHOR INFORMATION

Corresponding Author

* Tel.: +33 467 149 142. E-mail: anne.julbe@umontpellier.fr

Present Addresses

† Current address: Inorganic Membranes, MESA+ Institute for Nanotechnology, University of Twente, P.O. Box 217, 7500 AE Enschede, The Netherlands.

// Current address: Chemical and Process Engineering, University of Canterbury, 20 Kirkwood Ave, Upper Riccarton, Christchurch 8041, New-Zealand.

Author Contributions

The manuscript was written through contributions of all authors. All authors have given approval to the final version of the manuscript.

Notes

The authors declare no competing financial interest.

ACKNOWLEDGMENTS

ABBREVIATIONS

SILM, Supported Ionic Liquid Membrane; GILM, Grafted Ionic Liquid Membrane; $[Tf_2N]^-$, bis(trifluoromethanesulfonimide);

$[ImPE]^+$, 1-methyl-3-(3-(diethyl-phosphinyl)propyl)imidazolium; $[ImPEGPE]^+$, 1-methyl-3-(3-(diethylphosphinyl)-2–(2–(2–(2ethoxy)ethoxy)ethoxy)ethyl)-imidazolium; [bmim], 1-methyl-3-butylimidazolium; $[P_3mim]$, 1-(2-(2-(2-Methoxyethoxy)ethoxy)ethyl)-3-methylimidazolium; $[smmim][PF_6]$, 1-methyl-3-(1-trimethoxysilylmethyl) imidazolium hexafluorophosphate.

REFERENCES

1 Tomé, L.C.; Marrucho, I.M. Ionic liquid-based materials: a platform to design engineered CO_2 separation membranes. *Chem. Soc. Rev.* **2016**, *45(10)*, 2785-2824.

2 Cowan, M.G.; Gin, D.L.; Noble, R.D. Poly(ionic liquid)/Ionic Liquid Ion-Gels with high "free" ionic liquid content: platform membrane materials for CO_2/light gas separations. *Acc. Chem. Res.* **2016**, 49(4), 724-732.

3 Wang, J.; Luo, J.; Feng, S.; Li, H.; Wan, Y.; Zhang, X. Recent development of ionic liquid membranes. *Green Energy & Environment.* **2016**, *1(1)*, 43-61.

4 Hojniak, S.D.; Silverwood, I.P.; Khan, A.L.; Vankelecom, I.F.J.; Dehaen, W.; Kazarian, S.G.; Binnemans, K. Highly Selective Separation of Carbon Dioxide from Nitrogen and Methane by Nitrile/Glycol-Difunctionalized Ionic Liquids in Supported Ionic Liquid Membranes (SILMs). *J. Phys. Chem. B.* **2014**, *118(26)*, 7440–7749.

5 Hojniak, S.D.; Khan, A.L.; Hollo, O.; Kirchner, B.; Vankelecom, I.F.J.; Dehaen, W.; Binnemans, K. Separation of Carbon Dioxide from Nitrogen or Methane by Supported Ionic Liquid Membranes (SILMs): Influence of the Cation Charge of the Ionic Liquid. *J. Phys. Chem. B.* **2013**, *117(14)*, 15131−15140.

6 Close, J.J.; Farmer, K.; Moganty, S.S.; Baltus, R.E. CO_2/N_2 separations using nanoporous alumina-supported ionic liquid membranes: Effect of the support on separation performance. *J. Membrane. Sci.* **2012**, *390-391*, 201–210.

7 Vangeli, O.C.; Romanosa, G.E.; Beltsios, K.G.; Fokas, D.; Athanasekou, C.P.; Kanellopoulos, N.K. Development and characterization of chemically stabilized ionic liquid membranes-Part I: Nanoporous ceramic supports. *J. Membrane. Sci.* **2010**, *365,* 366–377.

8 Xin, B.; Hao, J. Imidazolium-based ionic liquids grafted on solid surfaces. *Chem. Soc. Rev.* **2014**, *43*, 7171–7187.

9 Guerrero, G.; Alauzun, J.G.; Granier, M.; Laurencin, D.; Mutin, P.H. Phosphonate coupling molecules for the control of surface/interface properties and the synthesis of nanomaterials. *Dalton Trans.* **2013**, *42*, 12569–12585.

10 Pizzoccaro, MA.; Drobek, M.; Petit, E.; Guerrero, G.; Hesemann, P.; Julbe, A. Design of Phosphonated Imidazolium-Based Ionic Liquids Grafted on γ-Alumina: Potential Model for Hybrid Membranes. *Int. J. Mol. Sci.* **2016**, *17*, 1212.

11 Finotello, A.; Bara, J.E.; Camper, D.; Noble, R.D. Room-Temperature Ionic Liquids: temperature dependence of gas solubility selectivity. *Ind. Eng. Chem. Res.* **2008**, *47(10),* 3453-3459.

12 Bara, J.E.; Gabriel, C.J.; Lessmann, S.; Carlisle, T.K.; Finotello, A.; Gin, D.L.; Noble, R.D. Enhanced CO_2 separation selectivity in oligo(ethylene glycol) functionalized room-temperature ionic liquids. *Ind. Eng. Chem. Res.* **2007***, 46(16)*, 5380-5386.

13 Freeman, B. D. Basis of Permeability/Selectivity Tradeoff Relations in Polymeric Gas Separation Membranes. *Macromolecules*. **1999**, *32(2)*, 375−380.

14 Baker, R. W. Membrane Technology and Applications, 2nd ed.; John Wiley & Sons: West Sussex, England, 2004.

15 Guerrero, G.; Mutin, P.H.; Vioux, A. Organically modified alumina by grafting and sol–gel processes involving phosphonate derivatives. *Chem. Mater.* **2001**, *13(11),* 4367-4373.

16 Scovazzo, P. Determination of the upper limits, benchmarks, and critical properties for gas separations using stabilized room temperature ionic liquid membranes (SILMs) for the purpose of guiding future research. *J. Membrane. Sci.* **2009**, *343(1-2)*, 199-211.

17 Bara, J.E.; Carlisle, T.K.; Gabriel, C.J.; Camper, D.; Finotello, A.; Gin, D.L.; Noble, R.D. Guide to CO_2 Separations in imidazolium-based Room-temperature Ionic Liquids. *Ind. Eng. Chem. Res.* **2009**, *48(6)*, 2739-2751.

18 Mu, ZG. ; Zhou, F.; Zhang, SX.; Liang, YM.; Liu, WM. Effect of the functional groups in ionic liquid molecules on the friction and wear behavior of aluminum alloy in lubricated aluminum-on-steel contact. *Tribology International.* **2005**, *38*, 725-731.

19 Mu, ZG.; Zhou, F.: Zhang, SX.; Liang, YM; Liu, WM. Preparation and Characterization of New Phosphonyl-Substituted Imidazolium Ionic Liquids. *Helvetica chimica acta.* **2004**, *87(10)*, 2549-2555.

20 Rout, A.; Venkatesan, K.A.; Srinivasan, T.G.; Vasudeva Rao, P.R. Unusual extraction of plutonium(IV) from uranium(VI) and americium(III) using phosphonate based task specific ionic liquid. *Radiochim. Acta.* **2010**, *98(8)*, 459-466.

21 Camper, D.; Bara, J.; Koval, C.; Noble, R.D. Bulk-fluid solubility and membrane feasibility of rmim-based room-temperature ionic liquids. *Ind. Eng. Chem. Res.* **2006**, *45(18)*, 6279-6283.

22 Bara, J.E.; Gabriel, C.J.; Lessmann, S.; Carlisle, T.K.; Finotello, A.; Gin, D.L.; Noble, R.D. Enhanced CO_2 separation selectivity in oligo(ethylene glycol) functionalized room-temperature ionic liquids. *Ind. Eng. Chem. Res.* **2007**, 46(16), 5380-5386.

23 Carlisle, T.K.; Bara, J.E.; Gabriel, C.J.; Noble, R.D.; Gin, D.L. Interpretation of CO_2 solubility and selectivity in nitrile-functionalized Room-Temperature Ionic Liquids using a group contribution approach. *Ind. Eng. Chem. Res.* **2008**, *47(18)*, 7005-7012.

24 Scovazzo, P.; Havard, D.; McShea, M.; Mixon, S.; Morgan, D. Long-term, continuous mixed-gas dry fed CO_2/CH_4 and CO_2/N_2 separation performance and selectivities for room temperature ionic liquid membranes. *J. Membrane. Sci.* **2009**, *327(1-2)*, 41-48.

25 Cadena, C.; Anthony, J.L.; Shah, J.K.; Morrow, T.I.; Brennecke, J.F.; Maginn, E.J. Why is CO_2 so soluble in imidazolium-based ionic liquids? *J. Am. Chem. Soc.* **2004**, *126(16)*, 5300-5308.

26 Hou, Y.; Baltus. R.E. Experimental Measurement of the Solubility and Diffusivity of CO_2 in Room-Temperature Ionic Liquids Using a Transient Thin-Liquid-Film Method. *Ind. Eng. Chem. Res.* **2007**, *46(24)*, 8166-8175.

27 Muldoon, M.J.; Aki, S.N.V.K.; Anderson, J.L.; Dixon, J.K.; Brennecke, J.F. Improving carbon dioxide solubility in ionic liquids. *J. Phys. Chem. B.* **2007**, *111(30)*, 185-92.

28 Klähn, M.; Seduraman, A. What Determines CO_2 Solubility in Ionic Liquids? A Molecular Simulation Study. *J. Phys. Chem. B.* **2015**, 119, 10066−10078.

29 Shannon, M.S.; Tedstone, J.M.; Danielsen, S.P.O.; Michelle, M.; Hindman, S.; Irvin, A.C.; Bara, J.E. Free volume as the basis of gas solubility and selectivity in imidazolium-Based Ionic Liquids. *Ind. Eng. Chem. Res.* **2012**, *51(15)*, 5565-5576.

30 Bara, J.E.; Carlisle, T.K.; Gabriel, C.J.; Camper, D.; Finotello, A.; Gin, D.L.; Noble, R.D. Guide to CO_2 Separations in imidazolium-based Room-temperature Ionic Liquids. *Ind. Eng. Chem. Res.* **2009**, *48(6)*, 2739-2751.

31 Horne, W.J.; Shannon, M.S.; Bara, J.E. Correlating fractional free volume to CO_2 selectivity in [Rmim][Tf$_2$N] ionic liquids. *J. Chem. Thermodynamics*. **2014**, *77*, 190-196.

32 Hu, Y.F.; Liu, Z.C.; Xu, C.M.; Zhang, X.M. The molecular characteristics dominating the solubility of gases in ionic liquids. *Chem. Soc. Rev*. **2011**, *40*, 3802-3823.

33 Ochsenfeld, C.; Kussmann, J.; Lambrecht, D.S.; Chapter 1: Linear-Scaling Methods in Quantum Chemistry. In Computational Chemistry, Ed., K.B. Lipkowitz and T.R. Cundari, Wiley-VCH, John Wiley & Sons, 2007, pp. 15.

34 Buijs, W.; Witkamp, GJ.; Kroon, M.C. Correlation between quantum chemically calculated LUMO energies and the electrochemical window of ionic liquids with reduction-resistant anions. *International Journal of Electrochemistry.* **2012**, *2012*, 1-6.

35 Morgan, D.; Fesrguson, L.; Scovazzo, P. Diffusivity of gases in room temperature ionic liquids: data and correlation obtained using a lag-time technique. *Ind. Eng. Chem. Res.* **2005**, *44(13)*, 4815-4823.

36 Ferguson, L: Scovazzo, P.; Solubility, diffusivity, and permeability of gases in phosphonium-based room temperature ionic liquids: data and correlations, *Ind. Eng. Chem. Res*., **2007**, *46(4)*, 1369-1374.

37 Condemarin, R.; Scovazzo, P. Gas permeabilities, solubilities, diffusivities, and diffusivity correlations for ammonium-based room temperature ionic liquids with comparison to imidazolium and phosphonium RTIL data. *Chem. Eng. J.* **2009**, *147(1)*, 51-57.

38 Höfft, O.; Bahr, S.; Kempter, V. Investigations with Infrared Spectroscopy on Films of the Ionic Liquid [emim][Tf_2N], *Langmuir.*, **2008**, *24(20)*, 11562-11566.

39 Freedman, L.D.; Doak, G.O. The preparation and properties of phosphonic acids. *Chemical Reviews*. **1957**, *57(3)*, 479-523.

40 Alam, T.M.; Jenkins, J.E. Chapter 10: HR-MAS NMR Spectroscopy in Material Science. In Advanced Aspects of Spectroscopy, Ed., M.A. Farrukh, GC University Lahore, Pakistan, 2012, pp. 279-306.

41 Drobek, M.; Motuzas, J.; Durand, V.; Duchateau, M.; Charmette, C.; Hertz, A.; Loubat, C.; Julbe, A. Evaluation of a new supercritical CO_2-assisted deposition method for preparing gas selective polymer/zeolite composite membranes. *J. Membrane. Sci.* **2013**, *429*, 428–435.

42 Albo, J.; Yoshioka, T.; Tsuru, T. Porous Al_2O_3/TiO_2 tubes in combination with 1-ethyl-3-methylimidazolium acetate ionic liquid for CO_2/N_2 separation. *Sep. Purif. Technol.* **2014**, 122, 440-448.

43 Gan, Q.; Rooney, D.; Xue, M.; Thompson, G.; Zou, Y. Supported ionic liquid membranes in nanopore structure for gas separation and transport studies. *J. Membr. Sci*. **2006**, *280*, 948–956.

44 Labropoulos, A.I.; Romanos, G.E.; Kouvelos, E.; Falaras, P.; Likodimos, V.; Francisco, M.; Kroon, M.C.; Iliev, B.; Adamova, G.; Schubert, T.J.S. Alkyl-methylimidazolium

Tricyanomethanide Ionic Liquids under Extreme Confinement onto Nanoporous Ceramic Membranes. *J. Phys. Chem. C.* **2013**, *117*, 10114−10127.

45 Tzialla, O.; Labropoulos, A.; Panou, A.; Sanopoulou, M.; Kouvelos, E.; Athanasekou, C.; Romanos, G. Phase behavior and permeability of Alkyl-Methyl-Imidazolium Tricyanomethanide ionic liquids supported in nanoporous membranes. *Sep. Purif. Technol.* **2014**, *135*, 22–34.

46 Robeson, L.M. The upper bound revisited. *J. Membrane. Sci.* **2008**, *320(1-2),* 390-400.

47 Merkel, T.C.; Lin, H.; Wei, X.; Baker, R. Power plant postcombustion carbon dioxide capture: An opportunity for membranes. *J. Membrane. Sci.* **2010**, 359(1-2), 126−139.

Table of Contents (TOC)/Abstract graphic